UNIVERSITY OF AMSTERDAM

UvA-DARE (Digital Academic Repository)

A revised model for circumstellar molecular emission

Groenewegen, M.A.T.

Publication date
1994

Published in
Astronomy & Astrophysics

Link to publication

Citation for published version (APA):
Groenewegen, M. A. T. (1994). A revised model for circumstellar molecular emission. *Astronomy & Astrophysics*, *290*, 531-543.

General rights
It is not permitted to download or to forward/distribute the text or part of it without the consent of the author(s) and/or copyright holder(s), other than for strictly personal, individual use, unless the work is under an open content license (like Creative Commons).

Disclaimer/Complaints regulations
If you believe that digital publication of certain material infringes any of your rights or (privacy) interests, please let the Library know, stating your reasons. In case of a legitimate complaint, the Library will make the material inaccessible and/or remove it from the website. Please Ask the Library: https://uba.uva.nl/en/contact, or a letter to: Library of the University of Amsterdam, Secretariat, Singel 425, 1012 WP Amsterdam, The Netherlands. You will be contacted as soon as possible.

UvA-DARE is a service provided by the library of the University of Amsterdam (https://dare.uva.nl)

Download date:09 Mar 2023

1994A&A...290..531G

Astron. Astrophys. 290, 531–543 (1994)

ASTRONOMY AND ASTROPHYSICS

A revised model for circumstellar molecular emission

M.A.T. Groenewegen[1,2]

[1] Astronomical Institute 'Anton Pannekoek', Kruislaan 403, NL-1098 SJ Amsterdam, The Netherlands
[2] Present address: Institut d'Astrophysique de Paris, 98bis Boulevard Arago, F-75014 Paris, France

Received 2 September 1993 / Accepted 8 March 1994

Abstract. A model is presented to calculate the line profiles of thermal emission of molecules in an expanding spherically symmetric circumstellar envelope. Special attention is given to the heating and cooling mechanisms which determine the kinetic temperature of the gas. The constraints that the presence of dust put on the molecular emission model are discussed. The following processes are found to have an effect of more than 10% on the integrated intensities (relative to a standard model): cooling by ^{13}CO and HCN in carbon stars, cooling by H_2O in oxygen-rich stars, and the location of the inner boundary of the molecular shell. The model including all physical features considered predicts CO(6–5) intensities which are 25% larger and CO(1–0) intensities which are 10% smaller than those of the standard model. Photoelectric heating can be the dominant source of heating in the outer layers, thereby determining the CO(1–0) intensity, depending on the beam size of the telescope and the efficiency of the shielding of UV radiation by dust.

Key words: circumstellar matter – stars: late type – radio lines: stars – stars: AGB, post-AGB

1. Introduction

Knowledge of the mass loss rate of AGB stars is crucial in understanding their evolution, because mass loss effectively determines the lifetime of a star on the AGB. The mass loss rate can be deduced from modelling the dust emission (e.g. Bedijn 1987; Schutte & Tielens 1989; Justtanont & Tielens 1992; Griffin 1993) or the molecular line emission. With regard to the latter, detailed models for individual stars have been proposed (IRC 10 216: Kwan & Hill 1977 (KH); Kwan & Linke 1982 (KL); Sahai 1987; Huggins et al. 1988; Truong-bach et al. 1991; U Cam: Sahai 1990; AFGL 2688: Truong-bach et al. 1990) or the convenient formula of Knapp & Morris (1985, KM) to calculate the mass loss rate has been widely used. Recently, Kastner (1992) presented an improved simple fit formula to determine the mass loss rate.

Send offprint requests to: M.A.T. Groenewegen at IAP address

The KM-formula is based on the assumption that the kinetic temperature derived for the infrared carbon star IRC 10 216 holds for other stars (including oxygen-rich ones) as well. It has been shown however that the kinetic temperature structure can be very different from that in IRC 10 216 (Sahai 1990; Jura et al. 1988 (JKO); Kastner 1992). Evidently, the kinetic temperature is strongly coupled to the molecular excitation calculation.

In this paper the heating and cooling mechanisms and the assumptions involved in calculating the kinetic temperature and the influence of them on the line profiles are investigated. The constraints that the presence of dust puts on molecular models are discussed. The main differences with the recent similar work of Kastner (1992) are in the exact treatment of the cooling by CO and the inclusion of the photoelectric effect.

In Sect. 2 all necessary theoretical ingredients are presented. In Sect. 3 the different components involved in the heating and cooling calculations and their influence on the line profiles are investigated. The results are discussed in Sect. 4.

2. Theory

2.1. The molecular excitation program

The model described by Morris et al. (1985) is used to calculate the level populations. The main assumptions are spherical symmetry and that the Sobolev approximation is valid (this presumes that the local linewidth is much smaller than the expansion velocity). The molecules are excited by: (1) collisions with H_2 molecules, (2) interaction with the 2.8 K background radiation, and (3) infrared radiation from a central blackbody of temperature T_{BB} and radius R_{BB} which leads to pumping from the $v = 0$ vibrational state into the $v = 1$ state.

The original model of Morris et al. was changed to incorporate the following effects:

1. In the original model the velocity law was used to calculate the radiation intensities in the vibrational and rotational lines but was not used in the density calculation. This was changed to give $n(r) \sim r^{-2}v^{-1}$ instead of the original $n(r) \sim r^{-2}$.

2. Helium is taken into account as a collision partner. The CO + He and HCN + He collisional cross sections are taken from Green & Chapman (1978) and Green & Thaddeus (1974),

© European Southern Observatory • Provided by the NASA Astrophysics Data System

1994A&A...290..531G

Table 1. The molecular constants

Molecule	$\mu_0(D)$	$\mu_{IR}(D)$	B (MHz)	D (MHz)	ω (cm^{-1})
^{12}CO	0.11	0.09	57635.97	0.1835	2170
^{13}CO	0.11	0.09	55101.02	0.1677	2075
HCN	2.99	0.10	44315.98	0.0872	715

Note. In Sect. 3 a value of $\mu_{IR} = 0.10$ is adopted for CO, in accordance with the value adopted by KH. μ_0 and μ_{IR} are the molecular dipole moment and the vibrational matrix element, and ω is the frequency of the $v = (0–1)$ transition.

respectively. The abundance $f_{He} = n(He)/n(H)$ is specified in the program.

3. In the original model the energy levels were calculated from $E(J) = BJ(J+1)$, where B is the rotational constant. Here, the second order term is included leading to $E(J) = BJ(J+1) - D(J(J+1))^2$.

4. In the original model the temperature structure of the gas in the envelope is specified. The most important change to the Morris et al. model is that in the present calculations the temperature structure is calculated in a self-consistent manner (see the next section).

The main input parameters are: the mass loss rate, the velocity law, the distance to the star, the photospheric abundance of the molecule of interest, the inner and outer radius of the envelope and the temperature and radius of the central blackbody to calculate the infrared intensities.

The calculations are performed using 99 gridpoints in the radial distance. Twenty-five rotational levels in both the $v = 0$ and $v = 1$ vibrational state are included. The line profiles are calculated at 48 velocity points. The molecular constants used are listed in Table 1. In the case of HCN, hyperfine splitting is neglected in the calculations.

2.2. The thermal balance equation for the gas

The kinetic temperature of the gas is given by (Goldreich & Scoville 1976 (GS), JKO):

$$\frac{dT}{dr} = (2-2\gamma)(1+0.5\epsilon)\frac{T}{r} + \frac{\gamma-1}{n(H_2)kv(r)(1+2f_{He})}(H-C) \quad (1)$$

where T is the gas temperature, γ the adiabatic index, $\epsilon = \frac{d\ln v}{d\ln r}$ the logarithmic velocity gradient, k the Boltzmann constant, H the total heating rate per unit volume and C the total cooling rate per unit volume.

Equation (1) can be simplified to:

$$\frac{dT}{dr} = -\beta\frac{T}{r} + f(r) \quad (2)$$

with as boundary condition $T(r_{inner}) = T_0$ and where β is assumed to be constant between two consecutive radial grid points. The solution of Eq. (2) is:

$$T(r) = T_0\left(\frac{r}{r_{inner}}\right)^{-\beta} + r^{-\beta}\int_{r_{inner}}^{r} f(r')(r')^{\beta}dr' \quad (3)$$

The main heating processes are dust-gas collisions and the photoelectric effect on grains. Heating due to cosmic rays and to the temperature difference between the gas and the dust are also included.

2.2.1. The heating processes

The heating rate per unit volume by dust-gas collisions is given by (KH, GS):

$$H_{dg} = 0.5\rho v_{dr}^3 n_d \sigma_d \quad (4)$$

where v_{dr} is the drift velocity of the dust w.r.t. the gas, n_d the dust grain number density and σ_d the dust cross section. This equation can be manipulated to give:

$$H_{dg} = 1.2254\,10^{-40} n(H_2)^2 \frac{\Psi(1+4f_{He})^2}{\rho_d a} \times \left(\frac{LQv(r)}{\dot{M}}\right)^{3/2} \frac{1}{1+\frac{v_{dr}}{v(r)}} \quad (\mathrm{erg\,s^{-1}\,cm^{-3}}) \quad (5)$$

with the drift velocity in km s^{-1} given by:

$$v_{dr} = 1.429310^{-4}\left(\frac{LQv(r)}{\dot{M}}\right)^{0.5} \quad (6)$$

where ρ_d is the dust grain density in gr cm^{-3}, a the grain size in μm, L the stellar luminosity in solar units, $\dot{M}$ the mass loss rate in $M_\odot$ yr^{-1}, Q the effective absorption coefficient (defined in Eq. 18), $v(r)$ the gas velocity in km s^{-1} and Ψ the dust-to-gas ratio. The term $1/(1+v_{dr}/v)$ was not included by KH (see Sahai 1990).

The gas and the dust have different temperatures. Therefore, heat can be exchanged between the two species. This process is insignificant in the energy balance for the dust (see e.g. Elitzur 1982) but may be important for the gas. The heating rate of the gas per unit volume may be written as (Burke & Hollenbach 1983):

$$H_{\Delta T} = n_H n_d \sigma_d \left(\frac{8kT}{\pi m_H}\right)^{0.5} \alpha_c 2k(T_d - T) \quad (7)$$

where α_c is the so-called accommodation coefficient and T_d the dust temperature. If all hydrogen is in molecular form (valid for $T \lesssim 1500$ K) this equation can be written as:

$$H_{\Delta T} = 2.00810^{-31} n(H_2)^2 \times \frac{\Psi(1+4\,f_{He})}{\rho_d a} T^{0.5}(T_d - T)\alpha_c \quad (\mathrm{erg\,s^{-1}\,cm^{-3}}) \quad (8)$$

The accommodation coefficient was determined by fitting the data in Fig. 4b of Burke & Hollenbach following the functional form in Hollenbach & McKee (1979):

$$\alpha_c = 0.35e^{-\sqrt{(T_d+T)/500}} + 0.1 \quad (9)$$

Note that when $T > T_d$, this process actually cools the gas.

© European Southern Observatory • Provided by the NASA Astrophysics Data System

1994A&A...290..531G

The heating rate per unit volume by the photoelectric effect can be written as (see de Jong 1977; Tielens & Hollenbach 1985; in erg s^{-1} cm^{-3}):

$$H_{\rm pe} = 1.3710^{-24} n({\rm H_2})(1+4f_{\rm He})\frac{\Psi}{\rho_{\rm d} a} G_0 \times \left(\frac{Y}{0.1}\right) {\rm e}^{-\tau_{0.1}} \left[\frac{(1-x)^2}{x} + x_{\rm k}\frac{x^2-1}{x^2}\right] \quad (10)$$

where $\tau_{0.1}$ is the dust optical depth from radius r to infinity at 0.1 μm, a is in micron, Y is the photoelectric yield of dust grains and G_0 is the UV flux in terms of the diffuse interstellar medium. The standard values $Y = 0.1$ and $G_0 = 1$ are used unless otherwise noted. The grain charge parameter x ($x = 0$ means neutral grains, $x = 1$ means grains with a maximum charge) is given by:

$$x^3 + (x_{\rm k} - x_{\rm d} + \gamma)x^2 - \gamma = 0 \quad (11)$$

with $x_{\rm k} = kT/13.6\,{\rm eV} = 6.33\,10^{-6}T$ and $x_{\rm d} = 0.442$ for the standard photoelectric threshold energy (6 eV) and where the dimensionless quantity γ is given by:

$$\gamma = 2.910^{-5} G_0 \left(\frac{Y}{0.1}\right) \frac{T^{0.5}}{n_{\rm e}} {\rm e}^{-\tau_{0.1}} \quad (12)$$

where $n_{\rm e}$ is the electron density. The reaction CO $\rightarrow$ O + C $\rightarrow$ O + C$^+$ + e$^-$ is the main provider of electrons. Mamon et al. (1988) showed that the abundance of neutral carbon is always less than the CO or C$^+$ abundance, so it is assumed that $n_{\rm e} = n_{\rm H_2} f_{\rm CO}(1 - X_{\rm CO})$, where $X_{\rm CO}$ (see Eq. 19) is the CO abundance relative to that at the inner radius.

The heating rate per unit volume by cosmic rays is given by (Goldsmith & Langer 1978):

$$H_{\rm cr} = 6.410^{-28} n({\rm H_2})(1+4f_{\rm He}) \quad ({\rm erg\,s^{-1}\,cm^{-3}}) \quad (13)$$

The uncertainty in the numerical coefficient is about a factor of 2.

2.2.2. The cooling processes

The cooling term C in Eq. (1) comprises molecular cooling by ^{12}CO, ^{13}CO, HCN, H_2 and H_2O. Other species are neglected. This is probably justified as other species like CS, SiO or SiS are underabundant by about an order of magnitude compared to HCN (e.g. Nyman et al. 1993). The cooling rate of ^{12}CO, ^{13}CO and HCN is calculated in the molecular excitation program from (Goldreich & Kwan 1974; de Jong et al. 1975; in erg s^{-1} cm^{-3}):

$$C_{\rm mol} = n_{\rm mol} \sum_{J=1}^{\infty} (2J+1) A_{J,J-1} \beta_{J,J-1} E_{J,J-1} \times \left(n_J - \frac{n_{J-1} - n_J}{\exp(E_{J,J-1}/kT_{\rm BG}) - 1}\right) \quad (14)$$

where $\beta_{J,J-1}$ is the escape probability of the rotational line radiation (see Castor 1970), $A_{J,J-1}$ the Einstein coefficient, $E_{J,J-1}$ the energy difference between levels J and $J-1$, n_J the fractional sub level population, $n_{\rm mol}$ the number of molecules per unit volume and $T_{\rm BG}$ the temperature of the cosmic background radiation.

The cooling rate by H_2 molecules, under the assumption of LTE, has been tabulated by Hartquist et al. (1980). The cooling rate per unit volume in the temperature range 100–900 K is well described by:

$$C_{\rm H_2} = n({\rm H_2}) 2.61110^{-21} (T/1000)^{4.74} \quad ({\rm erg/s/cm^3}) \quad (15)$$

The assumption of LTE is valid at densities $\gtrsim 10^6$ cm^{-3}. For a mass loss rate of $\sim 10^{-5}$ M$_\odot$ yr^{-1} and an expansion velocity of ~ 15 km s^{-1}, this occurs at distances $\lesssim 3\,10^{15}$ cm, or near the inner radius. Based on Eq. (15) it is expected that cooling by H_2 molecules is only important at high temperatures, or small radii, where the condition of LTE is fulfilled. At larger radii the condition of LTE is not fulfilled but it is expected that cooling by H_2 is not important. Therefore the assumption to use Eq. (15) in the entire envelope is not critical.

It is beyond the scope of this paper to include the effects of H_2O cooling in a self-consistent manner. Therefore the results available in the literature are used. Goldreich & Scoville (1976) developed a simple model to calculate the cooling rate by H_2O molecules. A similar model was used by Tielens (1983). Goldreich & Scoville presented their formula only for the explicit case they considered. Furthermore, they made some "non-essential simplifying approximations", which are neither necessary nor completely valid in all cases. Therefore, the formalism to calculate the cooling rate by H_2O is re-derived for the general case in Appendix A.

An important quantity is the water abundance. The water abundance is determined by the photodecay chain $H_2O \rightarrow$ OH+H $\rightarrow$ O+H+H. Other oxygen containing molecules like SO, SO_2 or O_2 always remain trace species. From chemical equilibrium studies which plot the H_2O, OH and O abundance as a function of radial distance it is derived that oxygen is mainly atomic at radii larger than twice the radius where the OH abundance reaches its maximum (Nejad & Miller 1988; Nercessian et al. 1989). The same conclusion is drawn from calculations which explicitly study the OH density profile as a function of mass loss rate and expansion velocity (Huggins & Glassgold 1982; Netzer & Knapp 1987). If the radius at which the OH profile peaks is taken from Netzer & Knapp, and it is assumed that oxygen is atomic at twice that distance, the maximum radius at which H_2O cooling can be important is given by:

$$r^{\rm max}({\rm H_2O}) = 35(\dot{M}/10^{-5}\,{\rm M_\odot\,yr^{-1}})^{0.7} \times (v/15\,{\rm km\,s^{-1}})^{-0.4} 10^{15}\,{\rm cm}. \quad (16)$$

The photospheric abundance of H_2O is determined by the carbon and oxygen supply available. During the first dredge-up on the red giant branch the carbon abundance is depleted to roughly two-thirds of the main-sequence value while the oxygen abundance remains unchanged with respect to the main-sequence values, which are assumed to be solar (H = 12.0, C = 8.60 and O = 8.93 on a logarithmic scale). If it is assumed that all carbon

© European Southern Observatory • Provided by the NASA Astrophysics Data System

1994A&A...290..531G

Table 2. The integrated intensity of ^{12}CO

Model	Integrated intensity and relative change (in %)					
	J = 1–0	2–1	3–2	4–3	5–4	6–5
1 Standard KH case (in K km s^{-1})	417	876	1220	1490	1705	1875
2 $v(r)$ and drift velocity consistent	−4	−7	−8	−9	−10	−10
3 Photoelectric heating $\tau_{0.1} = 2.3\,10^{17}$ cm/r	0	0	0	0	0	0
4 Cosmic ray heating	0	0	0	0	0	0
5 Heating due to gas-dust temperature difference	2	5	8	9	10	10
6 Cooling due to H_2	0	0	0	0	0	0
7 Cooling by H_2O included, $f_{H_2O} = 5\,10^{-4}$	−4	−11	−15	−17	−18	−20
8 Cooling by H_2O included, $f_{H_2O} = 1.2\,10^{-3}$	−5	−10	−13	−14	−15	−16
9 Cooling by ^{13}CO and HCN included	−4	−7	−9	−10	−11	−11
10 Helium, $f_{He} = 0.1$	−7	1	5	6	7	7
11 Outer radius set by photodissociation	0	0	0	0	0	0
12 Inner boundary T = 1000 K at $5R_*$, $\gamma = 5/3$	1	4	10	21	37	59
13 As model 12, $\gamma = 7/5$ when $T > 350$ K	1	4	10	22	39	62
14 $L = 5250\,L_\odot$, d = 100 pc	−41	−42	−40	−37	−36	−35
15 $L = 47250\,L_\odot$, d = 300 pc	−2	11	22	29	33	37
16 Mass loss times 2, dust opacity times 0.5	−34	−42	−41	−41	−40	−38
17 Mass loss times 0.5, dust opacity times 2	−11	12	35	51	61	67
18 Combined model	−10	−2	6	13	20	27

Note. The combined model includes: an inner radius at $4.2\,10^{14}$ cm with T = 850 K, $\gamma = 7/5$ when $T > 350$ K, the outer radius determined by photodissociation, the photoelectric effect included, an helium abundance of $n(He)/n(H) = 0.1$, cooling by H_2, ^{13}CO and HCN included, velocity law and drift velocity included in the heating calculation as well as heating by cosmic rays and due to the gas-dust temperature difference. Standard values for the mass loss rate, distance and dust opacity are used.

is locked up in CO and the remaining oxygen atoms are in water, typical CO and H_2O abundances are $f_{CO} = n(CO)/n(H_2) = 5.3\,10^{-4}$ and $f_{H_2O} = n(H_2O)/n(H_2) = 1.2\,10^{-3}$ when the star arrives on the AGB. On the AGB a star may add carbon to its envelope during the third dredge-up process after a thermal pulse. If a star has increased its C/O ratio to 0.7, the abundances change to $f_{CO} = 1.2\,10^{-3}$ and $f_{H_2O} = 5.1\,10^{-4}$. Since oxygen is partly depleted in the gas phase due to dust formation, the estimated water abundances are in fact upperlimits. The CO abundance is allowed to vary with radius (see Sect. 3.9). For simplicity we assume that the water abundance is constant between the inner radius and $r^{max}(H_2O)$. The importance of water cooling is investigated in Sect. 3.6.

2.3. How does dust affect the molecular excitation model?

Dust radiative transfer (DRT) models have been used to fit the spectral energy distribution (SED) of AGB stars and to derive mass loss rates (e.g. Bedijn 1987; Schutte & Tielens 1989; Groenewegen 1994). In fact, the mass loss rate can only be inferred if other quantities like the dust-to-gas ratio and the dust properties are known.

The quantity which is derived from fitting the SED is the dust optical depth:

$$\tau_\lambda = 5.405\,10^8 \frac{\dot{M}\Psi Q_\lambda/a}{r_c R_* v_d \rho_d} \quad (17)$$

where $\dot{M}$ is in $M_\odot\,yr^{-1}$, v_d the dust velocity in km s^{-1}, Ψ is the dust-to-gas ratio, Q_λ/a the dust absorption coefficient over the grain size in cm^{-1}, ρ_d the grain density in gr cm^{-3}, r_c the inner radius in stellar radii and R_* the stellar radius in solar units. The inner radius is determined by the temperature of the dust at the inner radius, T_c. The derivation of Eq. (17) assumes a constant dust velocity and mass loss rate. Near the dust condensation radius, which effectively determines the optical depth, the dust velocity is $v_d = v_{gas}(r_{condensation}) + v_{drift} \approx (0.8 - 0.9)v_{gas}(\infty) + (1 - 4 km\,s^{-1}) \approx v_{gas}(\infty)$ for typical parameter values. The assumption that the dust velocity equals the terminal velocity of the gas should be correct to within 10%. Comparing the parameters in Eq. (17) with the dominant heating source (Eq. 5) shows that $\dot{M}$, Ψ, ρ_d, a and Q cannot be varied independently but always must fulfil Eq. (17). JKO and Sahai (1990) also used the infrared fluxes to constrain their models, but their treatment is approximate and only uses the far-infrared fluxes. This method uses a fit to the entire SED.

The effective absorption efficiency Q (Eqs. 5–6) is calculated following Sahai (1990):

$$Q = \frac{\int F_\lambda Q_\lambda d\lambda}{\int F_\lambda d\lambda} \quad (18)$$

where F_λ is the emerging flux from the central star and the dust shell. In principle Q depends on the radius since F_λ is continuously changed by the dust emission but this is only important near the inner radius where the dust temperature changes

© European Southern Observatory • Provided by the NASA Astrophysics Data System

1994A&A...290..531G

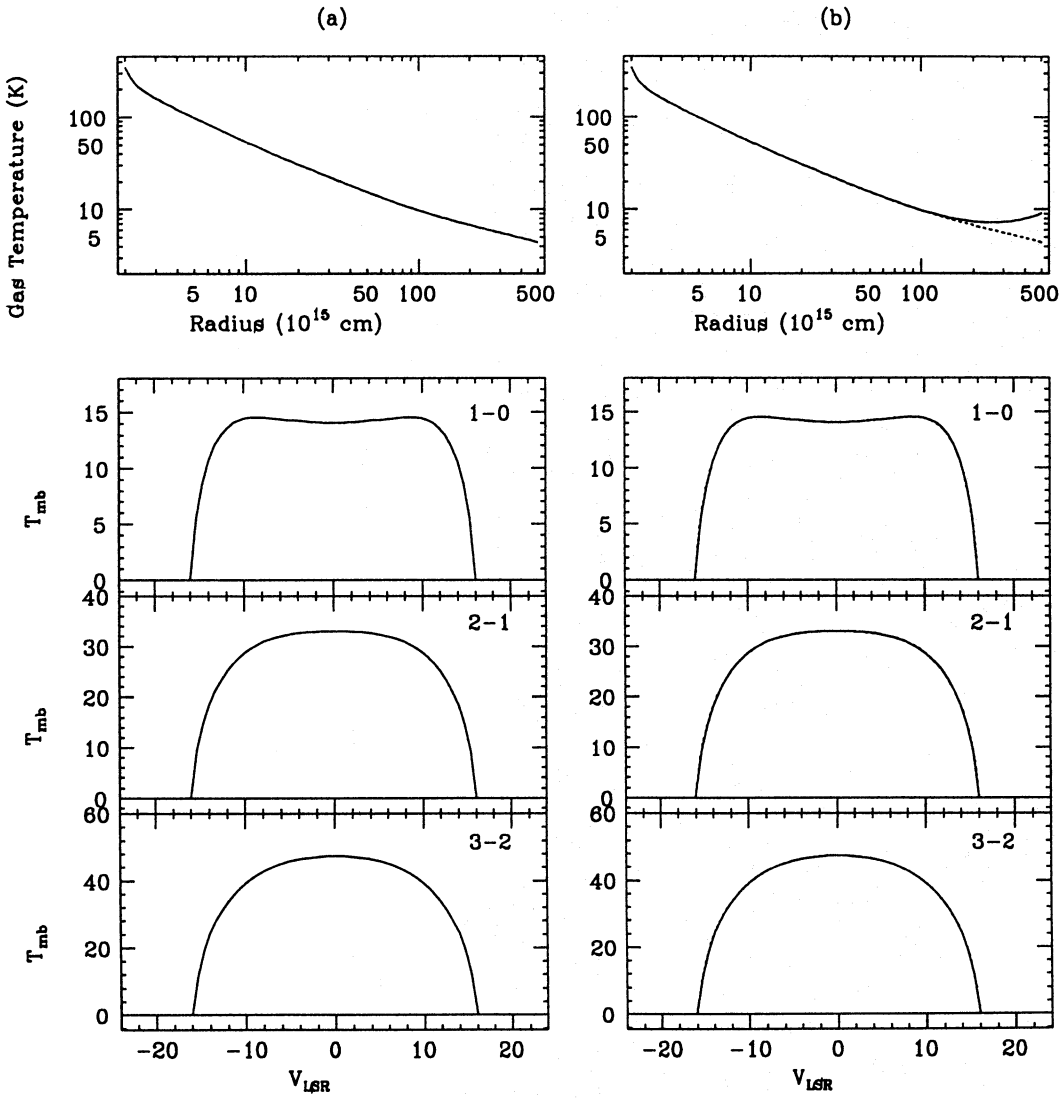

Fig. 1a and b. The temperature structure and CO line profiles for, **a** the standard Kwan & Hill (KH) case, and **b** when photoelectric heating is included. There is no change in the line profiles, only in the temperature structure. In panel **b** the standard KH case is represented by the dotted line. All profiles are calculated for a 30m telescope

rapidly (see Habing et al. 1994). The molecular emission originates from several tens to hundreds of stellar radii where F_λ is almost independent of the radial distance.

Radiative pumping of molecules is provided by thermal emission from hot dust close to the star. In molecular emission models this is represented by a blackbody of temperature $T_{\rm BB}$ and radius $R_{\rm BB}$. These quantities can be estimated from the DRT-models. At each gridpoint in the DRT-model the blackbody temperature of the radiation field is determined. In this way a realistic estimate of $T_{\rm BB}$ and $R_{\rm BB}$ is obtained. Finally, DRT-models provide $\tau_{0.1}$, which is needed to calculate the photoelectric heating (Eq. 10) and the dust temperature profile which is needed in the heating rate due to the gas-dust temperature difference (Eq. 7).

3. The relation between gas kinetic temperature and line profiles

In this section the influence of the different components involved in calculating the gas kinetic temperature are investigated. The model of KH for IRC 10 216 will be the reference case. The aim of this section is not to re-investigate IRC 10 216 but the KH results are the best documented regarding heating- and cooling rates and the temperature structure.

The parameters in the KH model are: luminosity L = 21 000 $L_\odot$, distance D = 200 pc, mass loss rate $\dot{M}$ = $2\,10^{-5}\,M_\odot\,{\rm yr}^{-1}$, dust-to-gas ratio Ψ = 0.01, grain radius a = 0.1 μm, grain density $\rho_{\rm d}$ = 1 gr cm^{-3}, absorption efficiency Q = 0.013. The inner boundary condition is T = 350 K at $2\,10^{15}$ cm. The adiabatic index is γ = 5/3. The CO abundance is $f_{\rm CO} = 8\,10^{-4}$ and is constant between $r_{\rm inner} = 2\,10^{15}$ and $r_{\rm outer} = 5\,10^{17}$ cm. The velocity law is $v(r)$ = 16.0(1 −

© European Southern Observatory • Provided by the NASA Astrophysics Data System

1994A&A...290..531G

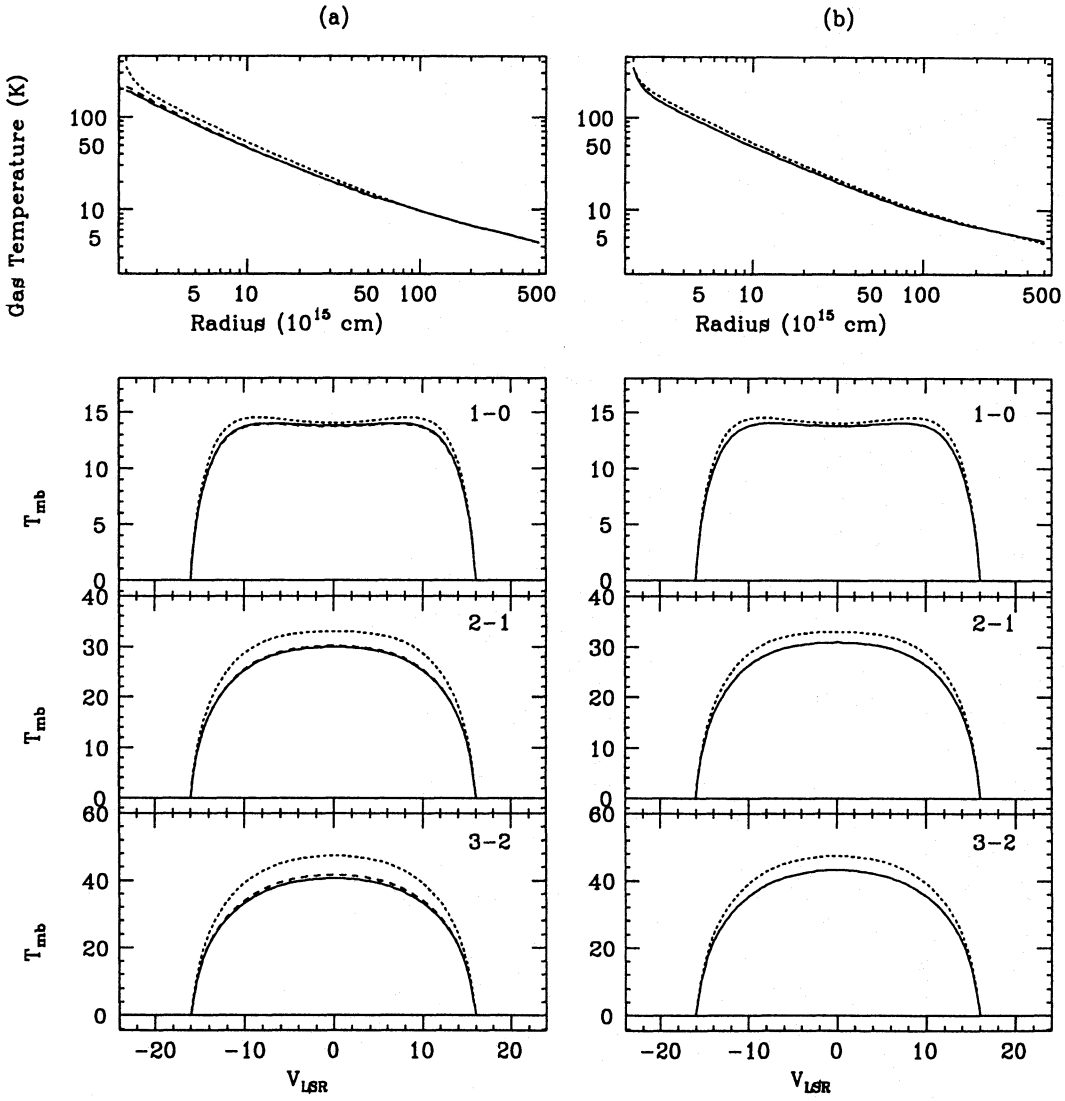

Fig. 2a and b. The temperature structure and CO line profiles when, **a** water cooling is included with an abundance $f_{H_2O} = 5\,10^{-4}$ (solid line) and $f_{H_2O} = 1.2\,10^{-3}$ (dashed line), and **b** cooling by ^{13}CO and HCN is included (without H_2O cooling). The dotted line indicates the standard KH case

$\frac{4\,10^{14}\,\mathrm{cm}}{r})^{0.5}\,\mathrm{km\,s^{-1}}$, but in the heating and cooling calculations KH assumed v = constant = $16.0\,\mathrm{km\,s^{-1}}$ and neglected the drift velocity (see Eq. 5). The central blackbody for calculating the infrared excitation is a 650 K blackbody of radius $6\,10^{14}$ cm for CO and a 300 K, $3\,10^{15}$ cm blackbody for HCN (again, all parameters taken from the KH model). Cooling by H_2, ^{13}CO and HCN is neglected and there is no helium or H_2O present. Heating by the photoelectric effect, cosmic rays and the temperature difference between the gas and the dust are neglected. For the effective temperature a value of $T_{\rm eff}$ = 2300 K is assumed (Ridgway & Keady 1988). The CO + H_2 and HCN + H_2 collision rates are taken from Green & Thaddeus (1974, 1976). KH did not explicitly state how they extrapolated the CO cross sections; I used the fit by de Jong et al. (1975).

The results of this standard case regarding the temperature structure and the CO(1–0), CO(2–1) and CO(3–2) profiles are shown in Fig. 1a. The profiles have been calculated for a 30m telescope (HPBW = 23″ at 115 GHz, corresponding to a linear radius of $3.4\,10^{16}$ cm at 200 pc). For the standard case I find a heating rate (neglecting the drift velocity in Eq. 5) per H_2 molecule of $7.5\,10^{-26}\,\mathrm{erg\,s^{-1}}$ and a cooling rate of $5.1\,10^{-26}\,\mathrm{erg\,s^{-1}}$ at $1\,10^{17}$ cm. KH find $7.4\,10^{-26}$ and $4.6\,10^{-26}\,\mathrm{erg\,s^{-1}}$, respectively. The gas temperature and CO(1–0) excitation temperature in the model are 9.73 and 8.39 K at $1\,10^{17}$ cm, 4.92 and 2.86 K at $4\,10^{17}$ cm. KH find 9.8 K, 8.1 K and 5.0 K, 2.8 K, respectively. The model results agree excellently with KH, the small differences are probably due to numerical details in the two codes.

In the following subsections the influence of several assumptions on the temperature structure and the CO line profiles is investigated. In Table 2 the changes in the integrated intensity ($\int T\mathrm{d}v$) relative to the standard case are tabulated for the low-

© European Southern Observatory • Provided by the NASA Astrophysics Data System

1994A&A...290..531G

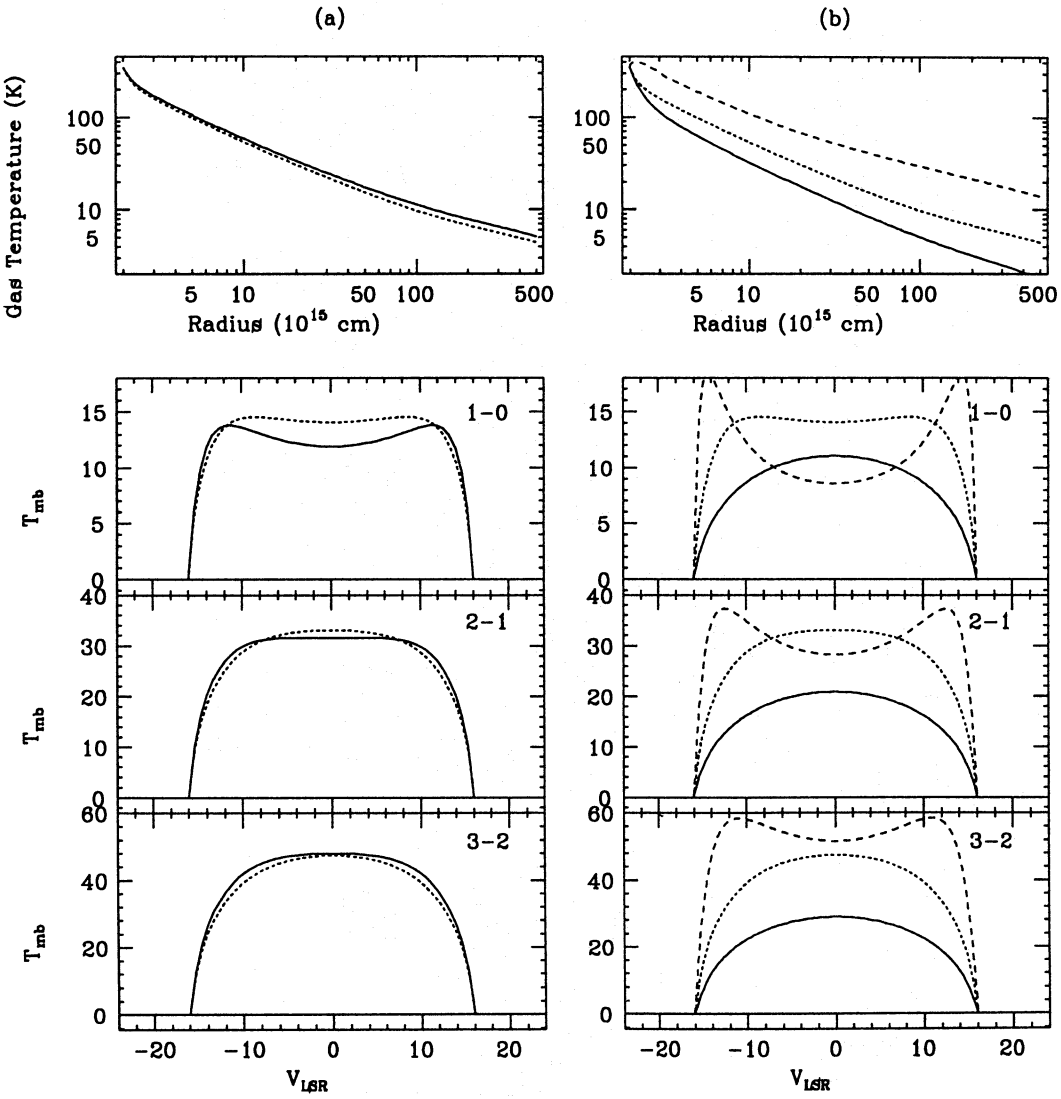

Fig. 3a and b. The temperature structure and CO line profiles when, **a** an helium abundance $f_{He} = 0.1$ is included, and **b** the mass loss rate and absorption efficiency are changed: $\dot{M} = 4\,10^{-5}\,M_\odot\,yr^{-1}$, $Q = 0.0065$ (solid line) or $\dot{M} = 1\,10^{-5}\,M_\odot\,yr^{-1}$, $Q = 0.026$ (dashed line). The dotted line is the standard KH case

est six transitions of ^{12}CO. In Figs. 1-4 the temperature structure and line profiles are shown for selected models.

3.1. The velocity law and drift velocity

KH assumed $v(r)$ = constant and neglected a term of the order $1/(1+v_{dr}/v)$ in the heating calculation. This results in an overestimate of the heating rate (Eq. 5). When the velocity law and the drift velocity are properly taken into account, lower temperatures and less emission are expected. The intensities are reduced by 5–10%.

3.2. Heating by the photoelectric effect

When UV radiation can penetrate the outer layers of the envelope the photoelectric effect on grains can become important. The heating rate is given by Eqs. 10–12. Since KH assumed a constant CO abundance, the electron density would be very small (as the net production of electrons by grains is negligible, cf. de Jong 1977) and there would be almost no photoelectric effect ($\gamma \rightarrow \infty, x \rightarrow 1, H_{pe} \rightarrow 0$). In order to get an estimate of the heating rate a value of $x = 0.7$ was assumed (Eq. 10). This gives a heating rate similar to the one adopted by KL and Truong-Bach et al. (1990). The parameter $\tau_{0.1}$ was estimated from Ridgway & Keady (1988) who derived a dust optical depth of 5.5 at 2 μm and an inner dust radius of $5R_*$ for IRC 10 216. Extrapolating the optical depth to 0.1 μm using the absorption efficiency of amorphous carbon (Rouleau & Martin 1991) which is appropriate for IRC 10 216 (Martin & Rogers 1987; Orofino et al. 1990; Griffin 1990), leads to an optical depth of 730 at the inner dust radius, or $\tau_{0.1} = 2.3\,10^{17}$ cm/r. This calculation neglects scattering. When scattering is important, which depends on the grain size, the optical depth at 0.1 μm will be larger. The line

© European Southern Observatory • Provided by the NASA Astrophysics Data System

1994A&A...290..531G

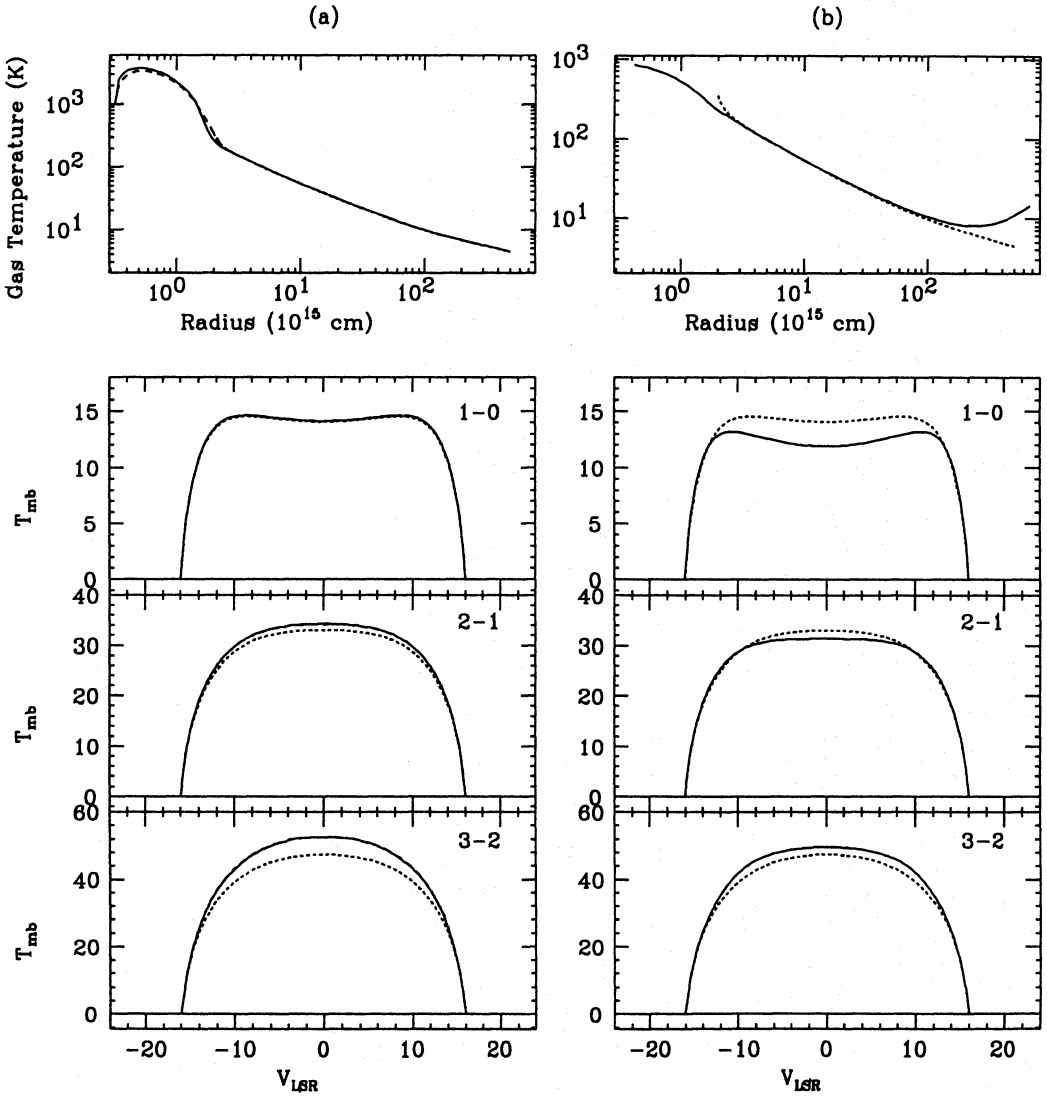

Fig. 4a and b. The temperature structure and CO line profiles when, **a** the inner boundary is T = 1000 K at 3.2 10^{14} cm with $\gamma = 5/3$ for all temperatures (solid line) and **b** the 'combined' model including all physics (see Sect. 3.12 for all details). The dotted line is the standard KH case

profiles and temperature structure are shown in Fig. 1b, which clearly illustrates the heating in the outer layers. *In this particular case*, photoelectric heating has a negligible effect on the line intensities because the beam size (3.4 10^{16} cm) is smaller than the region where the temperature is increased ($> 2.3\ 10^{17}$ cm). The ^{12}CO(1–0) integrated intensity is raised by 0.1%.

The photoelectric effect is a potentially important heating mechanism in the outer layers, but the effect on the (1–0) profile depends on the telescope beam size relative to the region where the UV radiation can effectively penetrate, which in turn depends on the uncertain contribution of scattering to the dust opacity at UV wavelengths. This means that the influence of the photoelectric effect on the line profiles is not easy to predict as it depends both on the distance to the object and the beam size of the telescope.

3.3. Heating by cosmic rays

This effect is totally negligible in this case. The temperature at the outer radius is raised by only 0.3 K compared to the standard case. The (1–0) integrated intensity is raised by 0.1%.

3.4. Heating by the gas-dust temperature difference

To estimate the effect of this process (Eq. 7), a dust temperature profile has to be adopted. From Griffin (1990) it is derived that for IRC 10 216 $T_{\rm d} = 530(r/10^{15}\,{\rm cm})^{-0.413}$ is a good approximation.

The effect is non-negligible. The intensities are raised by up to 10 percent. The ratio of the heating rates $H_{\Delta T}/H_{\rm dg}$ is 0.10 at the inner radius and 0.04 at 10^{17} cm.

© European Southern Observatory • Provided by the NASA Astrophysics Data System

1994A&A...290..531G

Table 3. The integrated intensity of ^{13}CO and HCN

Model		Integrated intensity (K km s^{-1})			
		$^{13}CO(1–0)$	$^{13}CO(2–1)$	$^{13}CO(3–2)$	HCN(1–0)
1	Standard KH case	34.0	112	195	181
18	Combined model	25.8	85.9	151	158
	Relative change	−24%	−23%	−23%	−13%

3.5. Cooling by H_2

Cooling by H_2 turns out to be negligible at the temperatures considered in the KH case ($T < 350$ K). The CO(6–5) integrated intensity is decreased by 0.2%. Since the cooling rate is a strong function of the temperature (see Eq. 15), it is expected that cooling by H_2 molecules may become important at smaller radii (higher temperatures).

3.6. Cooling by H_2O

In the case of oxygen-rich envelopes, H_2O cooling in the inner part of the envelope will be important. As the calculations in Sect. 3 are based on the parameters for the carbon star IRC 10 216 it should be clearly understood that this sub-section deals with a hypothetical oxygen-rich analog to IRC 10 216. We included H_2O cooling following the recipe outlined in Appendix A. From Eq. (16) it follows that $r^{max}(H_2O) = 55.4\,10^{15}$ cm. Models are calculated for abundances $f_{H_2O} = 5.0\,10^{-4}$ and $1.2\,10^{-3}$. The profiles are shown in Fig. 2a. The reduction in integrated intensity is substantial, up to 20% for the (6–5) transition (cf. Table 2). The reduction in the (1–0) line profile is much smaller, partly because all oxygen is in atomic form at the radii where the (1–0) emission arises. Most interestingly, the reduction in the CO intensities is less for $f_{H_2O} = 5.0\,10^{-4}$ than for $1.2\,10^{-3}$. This can be understood in terms how water cooling is treated (see Appendix A). The amount of water cooling depends on the product of the number density of water molecules and the difference between the gas temperature and the excitation temperature of the water molecules. For large water abundances, collisions of H_2O with H_2 dominate over radiative effects and tend to make both temperatures equal, so that with increasing water abundance the integrated CO line intensities reach a minimum and then increase again. From some test calculations it follows that the lowest CO line intensities are found for $3\,10^{-4} \lesssim f_{H_2O} \lesssim 8\,10^{-4}$, depending on the transition. For $f_{H_2O} = 5\,10^{-4}$, the ratio of the H_2O to the CO cooling rate is $\sim$ 64% at the inner radius, $\sim$ 36% at 10^{16} cm and $\sim$ 15% at $r^{max}(H_2O)$. The excitation temperature of the water molecules is about 2 K below the gas temperature.

3.7. Cooling by ^{13}CO and HCN

Cooling by ^{13}CO is expected to be more important than H_2O cooling at larger radii because the photodissociation radius of ^{13}CO is within 10% equal to that of ^{12}CO (Mamon et al. 1988). Therefore cooling by ^{13}CO will be important in the entire envelope and not, like water cooling, be limited to the inner envelope. In the following calculations an isotopic ratio $^{12}CO/^{13}CO = 35 (f_{^{13}CO} = 2.29\,10^{-5})$ and $f_{HCN} = 1.0\,10^{-5}$ are assumed. To be able to compare the relative importance of cooling by CO, HCN and ^{13}CO, the outer radius for HCN is also taken to be $5\,10^{17}$ cm[1]. The ^{12}CO line profiles, when ^{13}CO and HCN cooling are included, are shown in Fig. 2b. The emission is decreased by 4% (J = 1–0) to 11% (J = 6–5).

Although the abundance of the relevant species is ^{12}CO : ^{13}CO : HCN = 96.0 : 2.8 : 1.2, the contribution of the cooling rates is 81.2 : 8.1 : 10.7 at $2\,10^{15}$ cm, 81.2 : 11.8 : 7.0 at $1\,10^{16}$ cm and 89.4 : 8.8 : 1.8 at $1\,10^{17}$ cm. This clearly demonstrates that ^{13}CO and HCN are more important coolants than indicated by their relative abundances. This is due to the fact that the ^{12}CO lines are optically thick and line radiation cannot escape. When the ^{12}CO lines are optically thin (low $\dot{M}$, low f_{CO}) it is expected that the relative cooling rates are similar to the abundance ratios. This suggests that ^{13}CO cooling is a non-negligible coolant in the envelopes of J-type carbon stars, where $^{12}C/^{13}C \approx 5$–10.

3.8. Helium

All other parameters being equal, the presence of helium will increase the CO line intensities. The heating rate will remain the same, but the cooling rate will decrease since the CO number density is less, for a given mass loss rate, when helium is included. The profiles are shown in Fig. 3a for $f_{He} = 0.1$. The intensities are increased up to 7%. The change in lineshape is due to the increase in the size of the emission region relative to the beam size of the telescope.

3.9. The outer radius and photodissociation

KH assumed a constant CO abundance and outer radius. In reality, CO will be dissociated by the interstellar UV field and the CO abundance will decrease outward. Mamon et al. (1988) have investigated this effect and found that the CO abundance, relative to the value close to the star, can be approximated as:

$$X_{CO} = e^{-\ln(2)(r/r_{1/2})^{\alpha}} \quad (19)$$

[1] This is likely to be an overestimate. Observations of IRC 10 216 show that HCN is present to (at least) 22″ or $6.6\,10^{16}$ cm (Bieging et al. 1984). Therefore the contribution of HCN to the total radiative cooling rate at 10^{17} cm is even less than the 1.8% calculated above.

© European Southern Observatory • Provided by the NASA Astrophysics Data System

1994A&A...290..531G

where $r_{1/2}$ and α depend on $\dot{M}$ and v and are tabulated by Mamon et al. (1988). For the KH-case they are $r_{1/2} = 3.5\,10^{17}$ cm and $\alpha = 2.9$. The outer radius is set at the radius where the relative CO abundance drops to 1%, or $r_{\rm outer} = 6.7\,10^{17}$ cm. *In this particular case*, the change in the line profiles is negligible because the beamsize is much smaller than $r_{1/2}$.

3.10. Dust opacity and mass loss rate

Following the equation for the heating rate (Eq. 5) and the constraint put by DRT-models (Eq. 17) the largest change in the profiles can be expected by changing $\dot{M}$ and the dust opacity Q. Keeping $\dot{M}Q$ constant (cf. Eq. 17), $\dot{M} = 4\,10^{-5}\,{\rm M}_\odot\,{\rm yr}^{-1}$, $Q = 0.0065$ and $\dot{M} = 1\,10^{-5}\,{\rm M}_\odot\,{\rm yr}^{-1}$, $Q = 0.026$ are considered. The profiles are shown in Fig. 3b. Not only are the intensities changed due to the difference in heating, also the profiles are changed due to the change in the ratio of the beam size to the size of the emission region.

For both $\dot{M} = 1\,10^{-5}$ and $4\,10^{-5}\,{\rm M}_\odot\,{\rm yr}^{-1}$ the CO(1–0) emission is less than for $2\,10^{-5}\,{\rm M}_\odot\,{\rm yr}^{-1}$. As noted by Kastner (1992), the relation $T_{\rm mb} \sim \dot{M}$ of the KM-formula breaks down for high mass loss rates. If the mass loss rate is increased beyond a certain value, the decrease in heating rate is more important than the increase in the CO number density.

3.11. The inner boundary and the adiabatic index

The influence of the inner boundary condition on the temperature and the line profiles has not been properly investigated in the literature. KH assumed $T = 350$ K at $2\,10^{15}$ cm, JKO assumed 4000 K at $3\,10^{15}$ cm. Sahai (1990) points out that to take the radiative excitation into account properly, one needs to start the calculations at a few 10^{14} cm. Ideally one would use the central star as the inner boundary condition but this is not feasible. Shocks may have dissociated the molecules and ionized the hydrogen (Hinkle et al. 1982). From CO observations of χ Cyg there seems to be a stationary inner layer of ~ 800 K at $\sim 10R_*$ (Hinkle et al. 1982). A natural boundary condition seems to be the dust condensation radius since at this point the gas-dust heating process becomes effective.

For the standard KH case a model is calculated with the inner boundary condition modified to $T = 1000$ K at $r_{\rm inner} = 5R_* = 3.2\,10^{14}$ cm (Fig. 4a). In the velocity law ($v \sim (1 - c/r)^{0.5}$) the constant c is reduced from $4\,10^{14}$ cm (see Sect. 3.0) to $3\,10^{14}$ cm to make this inner boundary possible. As could be expected, the emission from the higher transitions is significantly increased (up to 60% for the $J = (6–5)$ transition).

An additional complication is that due to rotational excitation of H_2, the adiabatic index becomes less than 5/3 when $T \gtrsim 300$–1000 K (GS, JKO). To simulate this effect the same boundary condition as above, but with $\gamma = 7/5$ when $T > 350$ K was assumed. The effect of the change in adiabatic index is small ($\lesssim 3\%$) even at the high transitions.

3.12. Putting it all together: the combined model

The combined effect of the parameters discussed in Sects. 3.1–3.11 is investigated now. The standard value of the mass loss rate, distance and opacity are adopted. The velocity law and drift velocity are taken into account in the heating calculations, photoelectric heating is included with $\tau_{0.1} = 2.3\,10^{17}{\rm cm}/r$, heating by cosmic rays and the gas-dust temperature difference is included, photodissociation of ^{12}CO and ^{13}CO is included (Eq. 19) with $r_{1/2} = 3.5\,10^{17}$ cm, $\alpha = 2.9$ for both species (for simplicity the same values are used for HCN), cooling by H_2, ^{13}CO and HCN is included ($f_{^{13}{\rm CO}} = 2.29\,10^{-5}$, $f_{\rm HCN} = 1.00\,10^{-5}$), helium is included ($f_{\rm He} = 0.1$) and the inner boundary is set at $r_{\rm inner} = 4.2\,10^{14}$ cm. In Sect. 3.11 a temperature at the inner boundary of 1000 K was used. This value was probably too low as the temperature initially rises for larger radii (Fig. 4a). In the combined model the temperature at the inner radius is varied to give a smooth temperature profile near the inner radius. This results in an inner temperature of 850 K. The adiabatic index is $\gamma = 7/5$ when $T > 350$ K and $\gamma = 5/3$ when $T < 350$ K.

The resulting temperature structure and profiles are shown in Fig. 4b. Relative to the standard KH case, the $J = (1–0)$ and (2–1) intensities are reduced by up to 10% while the higher transitions ($J = 5–4$, 6–5) are increased by 20–25%. For completeness, the ^{13}CO and HCN profiles and intensities for the standard KH case and the combined model are given in Fig. 5 and Table 3. The ^{13}CO intensities are reduced by $\sim 25\%$ and the HCN(1–0) line by $\sim 15\%$.

4. Conclusions

A model is presented to calculate the line profiles of molecules in the expanding shell around a central star. The temperature structure is calculated in a self-consistent manner. Previous models usually only considered heating due to dust-gas collisions and cooling due to ^{12}CO (besides adiabatic cooling). Here, also additional heating and cooling processes are considered.

It is found that ^{13}CO and HCN can be important coolants in carbon stars. Cooling by H_2O is an important coolant in oxygen-rich stars. Photoelectric heating can be the dominant source of heating in the outer layers, thereby determining the CO(1–0) intensity, depending on the beam size of the telescope, the distance to the source and the efficiency of the shielding of UV radiation by dust.

For IRC 10 216 the effects of several physical modifications to the standard KH-model are investigated. The final model, including all physics considered, predicts integrated intensities which are 25% larger for the CO(6–5) transition and 10% smaller for the CO(1–0) transition. The changes for the low ^{13}CO transitions are $\sim 25\%$ smaller and for the HCN(1–0) transition about 15% smaller. The accuracy of observed line profiles is usually limited by calibration uncertainties (typically 10%). This suggests that the physical effects discussed in Sects. 3.1–3.11 have to be included in theoretical models for an accurate comparison with observations. The combination of simultane-

© European Southern Observatory • Provided by the NASA Astrophysics Data System

1994A&A...290..531G

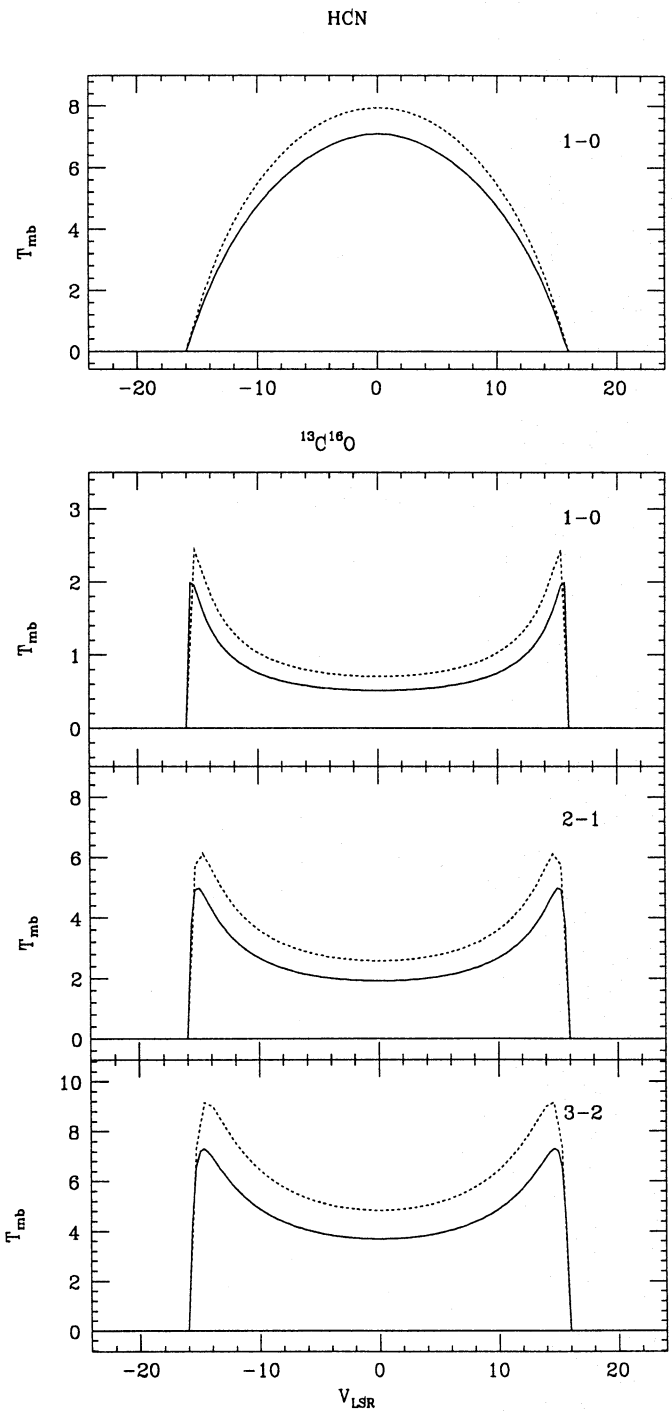

Fig. 5. The HCN and ^{13}CO line profiles for the combined model (solid line) and the standard KH case (dotted line)

ously fitting the spectral energy distribution and the molecular line emission profiles is potentially the most accurate method to determine the mass loss rate in AGB stars.

Acknowledgements. I thank Mark Morris for providing a copy of his numerical code and subsequent support and Xander Tielens for his comments on the treatment of water cooling and the photoelectric effect and for his interest in this project. Teije de Jong and René Oudmaijer are thanked for comments on the manuscript. The research of MG was supported under grant 782-373-030 by the Netherlands Foundation for Research in Astronomy (ASTRON), which is financially supported by the Netherlands Organisation for Scientific Research (NWO).

Appendix A: H_2O rotational cooling

I re-derive the equations to calculate the excitation temperature of a H_2O molecule and present the equation to calculate the cooling rate. This treatment is a generalization of the description by Goldreich & Scoville (1976, GS) and Tielens (1983). The calculation is based on the classical treatment of the H_2O molecule and assumes that all rotational levels in the ground vibrational state have the same excitation temperature T_x. With T_x determined, the cooling rate per unit volume is given by (GS Eq. 11, Tielens Eq. 15):

$$C_{H_2O} = n_{H_2}(1+\sqrt{2}f_{He})n_{H_2O} \times\langle\sigma v\rangle h\nu\left(e^{-h\nu/kT} - e^{-h\nu/kT_x}\right) \quad (A1)$$

where n_{H_2} and n_{H_2O} are the number densities of the respective molecules, f_{He} is the helium abundance relative to hydrogen and $\langle\sigma v\rangle$ is the H_2-H_2O inelastic collisional rate constant which is set to $\langle\sigma v\rangle = 2.0\,10^{-11}T^{1/2}\,\mathrm{cm^3\,s^{-1}}$ (GS). The He-H_2O collisional rate is assumed to be a factor $\sqrt{2}$ lower due to the difference in mass. The frequency ν is the classical value of the rotational frequency of an H_2O molecule whose rotational energy is $3kT_x/2$, or:

$$\nu = \nu_0 T_x^{1/2} \quad (A2)$$

In the derivation of the excitation temperature I closely follow GS. The idealised water molecule has three scalar levels, two rotational levels in the ground vibrational state and one rotational level in the excited vibrational state. The rate equations are given by (GS Eq. A1):

$$\begin{aligned}
\frac{dn_1}{dt} &= \beta_{21}A_{21}n_2 + (A_{31}+B_{31}J_{13})n_3 \\
&\quad -B_{13}J_{13}n_1 - C[n_1\exp(-h\nu_{21}/kT) - n_2] \\
\frac{dn_2}{dt} &= -\beta_{21}A_{21}n_2 + (A_{32}+B_{32}J_{23})n_3 \\
&\quad -B_{23}J_{23}n_2 + C[n_1\exp(-h\nu_{21}/kT) - n_2] \\
\frac{dn_3}{dt} &= B_{13}J_{13}n_1 + B_{23}J_{23}n_2 \\
&\quad -(A_{31}+B_{31}J_{13}+A_{32}+B_{32}J_{23})n_3 \\
n_1 + n_2 + n_3 &= n
\end{aligned} \quad (A3)$$

where $C = \langle\sigma v\rangle n_{H_2}(1+\sqrt{2}f_{He})$. The molecular levels are numbered 1, 2 and 3 in order of increasing energy. The net radiative decay rate is given by $\beta_{21}A_{21}$, where A_{21} is the spontaneous decay rate of level 2, and β_{21} is the probability that a photon escapes without further interaction. GS verified that the rotational transitions are optically thick and using the Sobolev approximation (Castor 1970), the term $\beta_{21}A_{21}$ is given by (GS Eq. A5):

$$\beta_{21}A_{21} = \frac{16\pi v(r)}{3r\lambda_{21}^3(n_1-n_2)}(1+0.5\epsilon) \quad (A4)$$

© European Southern Observatory • Provided by the NASA Astrophysics Data System

1994A&A...290..531G

where $\epsilon = \frac{\mathrm{d}\ln v}{\mathrm{d}\ln r}$. The profile averaged mean intensity for an optically thick line is given by (Castor 1970, GS Eq. A8):

$$J_{ij} = \epsilon W B_{\nu_{ij}}(T_\mathrm{e}) \tag{A5}$$

where $B_{\nu_{ij}}(T_\mathrm{e})$ is the Planck function for a temperature T_e and W is the dilution factor $W = 0.5(1-(1-(R_\mathrm{e}/r)^2)^{0.5})$. GS used the effective temperature and stellar radius for T_e and R_e, respectively. In other words, they neglected the influence of dust. The proper values for T_e and R_e are therefore T_BB and R_BB. Only in the case of low mass loss rates will T_BB and R_BB equal T_eff and R_*.

From the condition $\mathrm{d}n_3/\mathrm{d}t = 0$, assuming $A_{31} = A_{32}$ and defining $\frac{n_2}{n_1} \equiv \mathrm{e}^{-h\nu_{21}/kT_x}$, the following relation is derived:

$$\frac{n_3}{n_2} = \frac{1}{\frac{2}{\epsilon W} + \frac{1}{\mathrm{e}^{h\nu_{31}/kT_\mathrm{e}}-1} + \frac{1}{\mathrm{e}^{h\nu_{32}/kT_\mathrm{e}}-1}} \times \left(\frac{\mathrm{e}^{h\nu_{21}/kT_x}}{\mathrm{e}^{h\nu_{31}/kT_\mathrm{e}}-1} + \frac{1}{\mathrm{e}^{h\nu_{32}/kT_\mathrm{e}}-1}\right) \tag{A6}$$

Substituting Eq. (A6) in $\frac{1}{n_2}\frac{\mathrm{d}n_1}{\mathrm{d}t} = 0$ results in:

$$C\left(\exp(\frac{h\nu_{21}}{k}(\frac{1}{T_x}-\frac{1}{T}))-1\right) = \beta_{21}A_{21} + \epsilon W A_{31}\left(\frac{1}{2+\frac{\epsilon W}{\mathrm{e}^{h\nu_{31}/kT_\mathrm{e}}-1}+\frac{\epsilon W}{\mathrm{e}^{h\nu_{32}/kT_\mathrm{e}}-1}}\right) \times \left(\frac{1}{\mathrm{e}^{h\nu_{32}/kT_\mathrm{e}}-1} - \frac{\mathrm{e}^{h\nu_{21}/kT_x}}{\mathrm{e}^{h\nu_{31}/kT_\mathrm{e}}-1}\right) \tag{A7}$$

It can be verified that if $h\nu_{21}/kT_x \ll 1$, $h\nu_{21}/kT \ll 1$, $h\nu_{21}/kT_\mathrm{e} \ll 1$, $h\nu_{32}/kT_\mathrm{e} \gg 1$ and $h\nu_{31}/kT_\mathrm{e} \gg 1$ are fulfilled, Eq. (A7) simplifies to Eq. (A15) of GS, except for a factor 1/2 which seems to be missing in the last term of Eq. (A15) in GS.

If the excitation temperature derived from Eq. (A7) is to approximate the excitation temperature of the rotational levels of real water molecules, the values of ν_{21} and n (Eq. A3) must be chosen with some care. The appropriate value for n is given by (GS):

$$n = \frac{2(2J+1)}{Z_\mathrm{rot}} n_{\mathrm{H_2O}} \tag{A8}$$

where the rotational quantum number J and the partition function Z_rot are given by GS (Eq. A10–A12) and Tielens (Eq. A1–A2). They can be expressed as:

$$J = -0.5 + \sqrt{0.25 + j_0 T_x} \tag{A9}$$

$$Z_\mathrm{rot} = z_0 T_x^{3/2} \tag{A10}$$

The frequency ν_{21} is given by Eq. (A2). The constants[2] are $\nu_0 = 2.54\,10^{11}$ Hz, $j_0 = 7.39\,10^{-2}$, $z_0 = 8.38\,10^{-3}$. For the frequency $\nu_{31} = 1.13\,10^{14}$ Hz is assumed, corresponding to the strong transition at 2.66 μm (GS). The frequencies are related through $\nu_{32} = \nu_{31} - \nu_{21}$. The Einstein coefficient equals $A_{31} = 34\,\mathrm{s}^{-1}$ (GS). Substituting Eq. (A4) in Eq. (A7), using Eqs. (A2, A8, A9, A10) and the continuity equation results in:

$$\begin{aligned} &2.0\,10^{-11}T^{0.5}n_{\mathrm{H_2}}(1+\sqrt{2}f_\mathrm{He})\left(\exp\left(\frac{h\nu_{21}}{k}\left(\frac{1}{T_x}-\frac{1}{T}\right)\right)-1\right) \\ &= \frac{16\pi}{6} z_0 \left(\frac{\nu_0}{c}\right)^3 v(r)(1+0.5\epsilon)\frac{T_x^3}{\sqrt{1+4j_0T_x}} \\ &\times \left(\frac{1+\mathrm{e}^{-h\nu_{21}/kT_x}+\frac{n_3}{n_2}}{1-\mathrm{e}^{-h\nu_{21}/kT_x}}\right) \Big/ (r f_{\mathrm{H_2O}} n_{\mathrm{H_2}}) \\ &+\epsilon W A_{31}\left(\frac{1}{2+\frac{\epsilon W}{\mathrm{e}^{h\nu_{31}/kT_\mathrm{e}}-1}+\frac{\epsilon W}{\mathrm{e}^{h\nu_{32}/kT_\mathrm{e}}-1}}\right) \\ &\times \left(\frac{1}{\mathrm{e}^{h\nu_{32}/kT_\mathrm{e}}-1} - \frac{\mathrm{e}^{h\nu_{21}/kT_x}}{\mathrm{e}^{h\nu_{31}/kT_\mathrm{e}}-1}\right) \end{aligned} \tag{A11}$$

where $n_{\mathrm{H_2}}$ is the number density of H_2 molecules at radius r. For a given mass loss rate, velocity law, effective temperature, water abundance and gas temperature, Eq. (A11) can be solved for T_x at any radius r. Having determined T_x, the water cooling rate is determined from Eq. (A1).

References

Bedijn P.J., 1987, A&A 186, 136
Bieging J.H, Chapman B., Welch W.J., 1984, ApJ 285, 656
Burke J.R., Hollenbach D.J., 1983, ApJ 265, 223
Castor J.I., 1970, MNRAS 149, 111
Elitzur M., 1982, ApJ 262, 189
Goldreich P., Kwan J., 1974, ApJ 189, 444
Goldreich P., Scoville N., 1976, ApJ 205, 144 (GS)
Goldsmith P.F., Langer W.D., 1978, ApJ 222, 881
Green S., Chapman S., 1978, ApJS 37, 169
Green S., Thaddeus P., 1974, ApJ 191, 653
Green S., Thaddeus P., 1976, ApJ 205, 766
Griffin I.P., 1990, MNRAS 247, 591
Griffin I.P., 1993, MNRAS 260, 831
Groenewegen M.A.T., 1994, A&A (in press)
Habing H.J., Tignon J., Tielens A.G.G.M., 1994, A&A 286, 523
Hartquist T.W., Oppenheimer M., Dalgarno A., 1980, ApJ 236, 182
Hinkle K.H., Hall D.N.B., Ridgway S.T., 1982, ApJ 252, 697
Hollenbach D.J., McKee C.F., 1979, ApJS 41, 555
Huggins P.J., Glassgold A.E., 1982, AJ 87, 1828
Huggins P.J., Olofsson H., Johansson L.E.B., 1988, ApJ 332, 1009

[2] Note that in some equations in GS the factor h should read $\hbar$ and that the quoted moments of inertia are a factor 2π too high, although the quoted values for j_0 and z_0 are correct. The value for ν_0 seems to be a factor 2 too low in GS. The values for j_0, z_0 and ν_0 are based on the more recent values of $I_1 = 1.004\,10^{-40}$, $I_2 = 1.928\,10^{-40}$ and $I_3 = 3.017\,10^{-40}$ gr cm^2. Furthermore, GS make the approximation $M/\hbar = J$ while the correct expression is $M/\hbar = \sqrt{J(J+1)}$. This is why the value for j_0 approximately is the square of the value quoted by GS.

© European Southern Observatory • Provided by the NASA Astrophysics Data System

1994A&A...290..531G

de Jong T., Chu S.I., Dalgarno A., 1975, ApJ 199, 69
de Jong T., 1977, A&A 55, 137
Jura M., Kahane C., Omont A., 1988, A&A 201, 80 (JKO)
Justtanont K., Tielens A.G.G.M., 1992, ApJ 389, 400
Kastner J.H., 1992, ApJ 401, 337
Knapp G.R., Morris M., 1985, ApJ 292, 640
Kwan J., Hill F., 1977, ApJ 215, 781 (KH)
Kwan J., Linke R.A., 1982, ApJ 254, 587 (KL)
Mamon M., Glassgold A.E., Huggins P.J., 1988, ApJ 328, 797
Martin P.G., Rogers C, 1987, ApJ 322, 374
Morris M., Lucas R., Omont A., 1985, A&A 142, 107
Nejad L.A.M., Miller T.J., 1988, MNRAS 230, 79
Nercessian E., Guilloteau S., Omont A., Benayoun J.J., 1989, A&A 210, 225
Netzer N., Knapp G.R., 1987, ApJ 323, 734
Nyman L.-A., 1993, A&A 269, 377
Orofino V., Colangeli L., Bussoletti E., Blanco A., Fonti S., 1990, A&A 231, 105
Ridgway S.T., Keady J.J., 1988, ApJ 326, 843
Rouleau F., Martin P.G., 1991, ApJ 377, 526
Sahai R., 1987, ApJ 318, 809
Sahai R., 1990, ApJ 362, 652
Schutte W.A., Tielens A.G.G.M., 1989, ApJ 343, 369
Tielens A.G.G.M., 1983, ApJ 271, 702
Tielens A.G.G.M., Hollenbach D., 1985, ApJ 291, 722
Truong-Bach, Morris D., Nguyen-Q-Rieu, Deguchi S., 1990, A&A 230, 431
Truong-Bach, Morris D., Nguyen-Q-Rieu, 1991, A&A 249, 435

© European Southern Observatory • Provided by the NASA Astrophysics Data System